Received: 26 February 2023 | Revised: 9 May 2023 | Accepted: 31 May 2023

DOI: 10.1002/acm2.14073

JOURNAL OF APPLIED CLINICAL MEDICAL PHYSICS

RADIATION ONCOLOGY PHYSICS

Three-dimensional assessment of interfractional cervical and uterine motions using daily magnetic resonance images to determine margins and timing of replanning

Yukako Kishigami[1] | Mitsuhiro Nakamura[1] | Megumi Nakao[2] | Hiroyuki Okamoto[3] | Ayaka Takahashi[4] | Hiroshi Igaki[4]

[1]Department, of Advanced Medical Physics, Graduate School of Medicine, Kyoto University, Kyoto, Japan

[2]Department of Biomedical Engineering and Intelligence, Graduate School of Medicine, Kyoto University, Kyoto, Japan

[3]Radiation Safety and Quality Assurance Division, National Cancer Center Hospital, Tokyo, Japan

[4]Department of Radiation Oncology, National Cancer Center Hospital, Tokyo, Japan

Correspondence
Mitsuhiro Nakamura, Department of Advanced Medical Physics, Graduate School of Medicine, Kyoto University, 53 Kawahara-cho, Shogoin, Sakyo-ku, Kyoto 606-8507, Japan.
Email: m_nkmr@kuhp.kyoto-u.ac.jp

Funding information
JSPS KAKENHI, Grant/Award Number: 22H03021

Abstract

Purpose: This study was conducted to determine the margins and timing of replanning by assessing the daily interfractional cervical and uterine motions using magnetic resonance (MR) images.

Methods: Eleven patients with cervical cancer, who underwent intensity-modulated radiotherapy (IMRT) in 23–25 fractions, were considered in this study. The daily and reference MR images were converted into three-dimensional (3D) shape models. Patient-specific anisotropic margins were calculated from the proximal 95% of vertices located outside the surface of the reference model. Population-based margins were defined as the 90th percentile values of the patient-specific margins. The expanded volume of interest (expVOI) for the cervix and uterus was generated by expanding the reference model based on the population-based margin to calculate the coverage for daily deformable mesh models. For comparison, $expVOI_{conv}$ was generated using conventional margins: right (R), left (L), anterior (A), posterior (P), superior (S), and inferior (I) were (5, 5, 15, 15, 10, 10) and (10, 10, 20, 20, 15, 15) mm for the cervix and uterus, respectively. Subsequently, a replanning scenario was developed based on the cervical volume change. $ExpVOI_{ini}$ and $expVOI_{replan}$ were generated before and after replanning, respectively.

Results: Population-based margins were (R, L, A, P, S, I) of (7, 7, 11, 6, 11, 8) and (14, 13, 27, 19, 15, 21) mm for the cervix and uterus, respectively. The timing of replanning was found to be the 16th fraction, and the volume of $expVOI_{replan}$ decreased by >30% compared to that of $expVOI_{ini}$. However, margins cannot be reduced to ensure equivalent coverage after replanning.

Conclusion: We determined the margins and timing of replanning through detailed daily analysis. The margins of the cervix were smaller than conventional margins in some directions, while the margins of the uterus were larger in almost all directions. A margin equivalent to that at the initial planning was required for replanning.

KEYWORDS
cervical cancer, daily MR images, interfractional variations, margin, replanning

1 | INTRODUCTION

In recent years, intensity-modulated radiotherapy (IMRT) has been widely used to treat cervical cancer as it significantly reduces acute gastrointestinal and genitourinary (GU) toxicities and chronic GU toxicity in patients compared to three-dimensional (3D) conformal radiotherapy.[1,2] However, interfractional variations, including tumor regression and target positional change, are the most important issues that must be addressed owing to the risks of tumor under-dosing and/or normal tissue over-dosing.[3–16]

Although many researchers have studied such variations, there has been a lack of daily observation, individual assessment distinguishing the cervix and uterus with high-contrast medical images, and 3D evaluations.[8–16] Several researchers have reported margins for cervical cancer without daily observations or individual assessments, and all of them used two-dimensional (2D) evaluations.[8–12] Bondar et al. designed a 3D model to predict the shape and position of the cervix and uterus. However, they did not perform daily imaging and did not assess the cervix or uterus separately.[13] Although some studies revealed the effectiveness of replanning against tumor regression, they were still not based on daily MR images.[14–16] Online adaptation systems have emerged in recent years. Although the effectiveness of target coverage with a smaller margin and OAR sparing has been proven,[17,18] several human and time resources are required. Moreover, the ownership rate of online adaptation systems is low worldwide. Online adaptive radiotherapy with library plans is one approach for improving OAR sparing.[19,20] However, such a system is not commercially available. Therefore, the appropriate margin and timing of replanning are important issues that need to be addressed for cervical radiotherapy. To address the issues, a precise assessment of interfractional movement is required.

This study introduced two completely different techniques. First, a 3D evaluation approach was developed to assess organ motions by applying a shape model to express variations in their shape.[21,22] Second, daily MR images acquired from an MR-guided radiotherapy (MRgRT) system were used. The MRgRT system provided daily high-contrast images, thereby allowing independent motion analysis of the cervix and uterus. This study was aimed at determining the margins and timing of replanning assessing interfractional cervical and uterine motions three-dimensionally with daily MR images.

2 | MATERIALS AND METHODS

2.1 | Patients and data preparation

For this study, we considered 11 patients with cervical cancer who underwent MR-guided IMRT using the ViewRay MRIdian (Viewray Inc., Oakwood Village, OH, USA) (Table 1). The pulse sequence used for volumetric imaging was a True Fast Imaging with Steady State Precession sequence. The slice thickness and pixel dimensions of the MR images were 3 mm and 1.5 mm × 1.5 mm, respectively. All patients were asked to urinate and defecate and were then asked to drink 300 mL of water 1 h before entering the treatment room. The daily MR images of each patient were acquired before beam delivery and co-registered to the planned MR images (reference) based on the bony structure. Thereafter, the uterus, cervix, rectum, and bladder were manually delineated by a single radiation oncologist. The contours were converted to mesh file formats using a commercially available system (ITEM Viewer Planning and Assistant System; ITEM Corporation, Osaka, Japan). Each mesh comprised a unique number of vertices and meshes. Therefore, the surfaces of all acquired meshes were resampled such that we acquired 400 vertices and 796 triangular meshes. As a result, we obtained a point-to-point correspondence. The details have been described elsewhere.[21,22] This study was approved by the institutional review board (approval number: 2020-556).

2.2 | Calculation of displacement

Figure 1 shows the flowchart of this study. The daily displacements of the cervix and uterus were acquired as follows: 400 displacement vectors of each corresponding vertex were obtained between each daily shape model and the reference model. The mean displacement was computed by averaging over 400 displacement vectors, defined as the displacement of the day. The cervical volume change was calculated as the percentage of daily cervical volume compared to the reference cervical volume to acquire the trend of cervical volume change. Additionally, Pearson's correlation coefficients were calculated between the cervical volume change and displacement of the cervix or uterus.

2.3 | Computation of patient-specific anisotropic margins

The anisotropic margin was computed from the vertices of the daily shape models displaced outside the surface of the reference model (outside vertices). First, the origin was set at the centroid of the reference model, and the outside vertices (1^{st}–23^{rd} or 25^{th}) were identified. Subsequently, a vector drawn from the surface of the reference model to the vertex was obtained for each outside vertex. Then, the vectors were decomposed along six directions around the origin: right (R), left (L), anterior (A), posterior (P), superior (S), and inferior (I). Lastly, we computed the patient-specific margins covering the proximal

TABLE 1 Patient characteristics.

Pt#	Age (y.o.)	Pathology	TNM	Stage	Chemo	Dose (Gy/fr)	Cx (cm^3)[a1]	Ut (cm^3)[a1]
1	63	Ad	T3bN1M0	IIIB	–	46/25	15.9	102.1
2	35	SCC	T3bN1M0	IIIB	CDDP	45/25	103.8	77.9
3	65	SCC	T1b1N0M0	IB	–	45/25	9.9	3.6
4	73	SCC	T3bN1M0	IIIB	–	46/23	15.5	27.2
5	76	SCC	T3bN1M0	IIIB	CDDP	45/25	103.5	78.9
6	67	SCC	T2bN1M0	IIB	CDDP	45/25	38.8	16.9
7	71	SCC	T2bN1M0	IIB	CBDCA	45/25	29.6	33.4
8	70	SCC	T2bN0M0	IIB	CDDP	45/25	20.3	13.6
9	47	SCC	T3bN1M0	IIIB	CDDP	45/25	46.9	82.9
10	88	SCC	T1b1N0M0	IB	–	45/25	13.7	21.7
11	44	SCC	T3bNxM0	IIIB	CBDCA	45/25	45.0	91.2

Abbreviations: Ad, adenocarcinoma; CBDCA, carboplatin; CDDP, cisplatin; Chemo, chemotherapy; Cx, cervix; Pt#, patients; SCC, squamous cell carcinoma; Ut, uterus.
[a]1: Volume at treatment planning (cm^3).

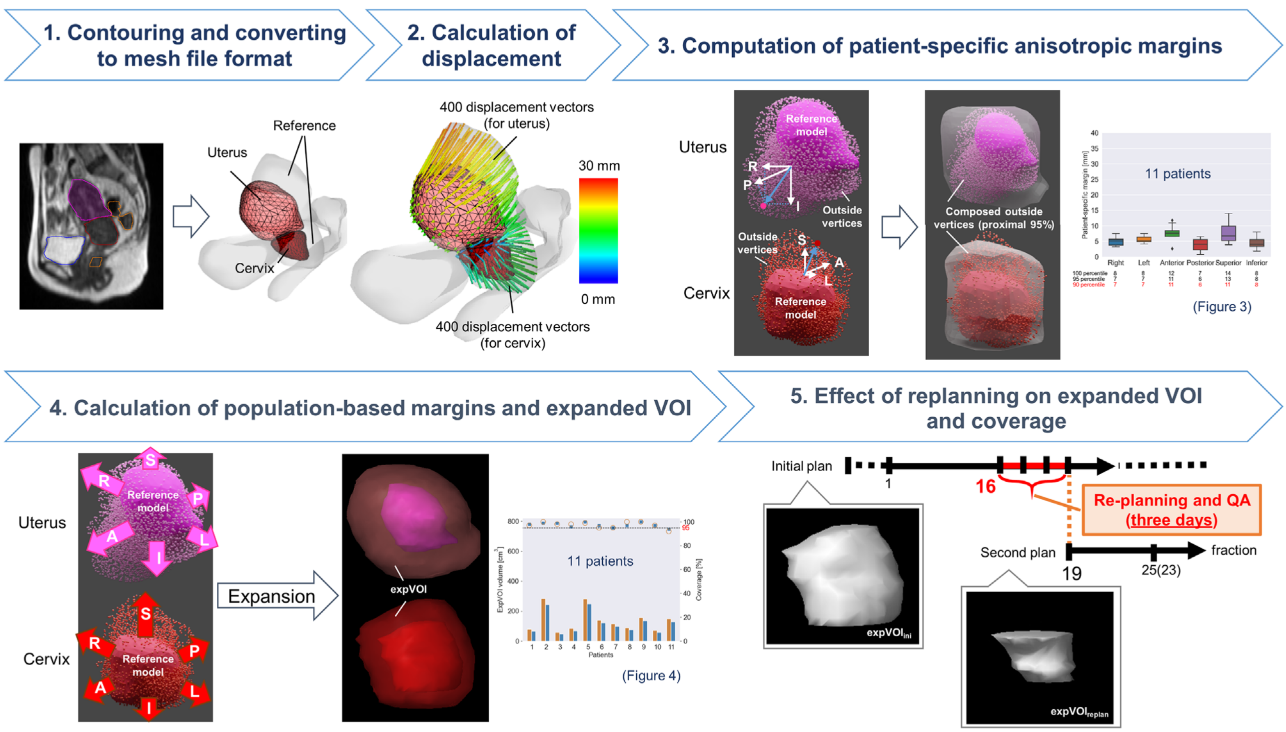

FIGURE 1 Schematic flow of this study.

95% of the outside vertices for all 11 patients based on the lengths of the decomposed vectors in each direction.

2.4 | Calculation of population-based margins and expanded VOI

The 90[th] percentile values of the patient-specific margins were defined as the population-based margins in each direction. First, the expanded volume of interest (expVOI) was generated by expanding the reference model depending on the population-based margins in each direction, which was regarded as a surrogate for a planning target volume. Next, the volume and coverage probabilities of the expVOI were calculated for all patients. The coverage was calculated as the ratio of the vertices of the daily shape models located within the expVOI to the outside vertices. For comparison, $expVOI_{conv}$ was generated by adding conventional margins to the reference cervix and uterus, and the volume of $expVOI_{conv}$ and the coverage probabilities were calculated. Conventional margins (R, L, A, P, S, I) of (5, 5, 15, 15, 10, 10) and (10, 10, 20, 20, 15, 15) mm were used for the cervix and uterus, respectively. The clinical target volume (CTV) margins suggested by Khan et al.[12] were used as conventional margins for the uterus and margins 5 mm smaller than conventional margins for the uterus were used as conventional margins for the cervix.

2.5 | Effect of replanning on expanded volume and coverage

A replanning scenario was developed based on the trend in cervical volume change. When the median cervical volume fell below 50% for the first time, the date was set as the new reference date (X^{th} fraction). The replan was simulated based on the shape of the cervix and uterus in the X^{th} fraction. Considering the time required for optimization and quality assurance, the second plan was assumed to start at the $(X + 3)^{th}$ fraction.

Two patient-specific margins were computed before and after replanning. Before replanning, patient-specific margins were computed to cover 95% of the outside vertices (1^{st}—$[X + 2]^{th}$), whereas after replanning, they were computed to cover 95% of the outside vertices ($[X + 3]^{th}$—23^{rd} or 25^{th}). Population-based margins were determined as the 90^{th} percentile values of each patient-specific margin. Two expVOIs ($expVOI_{ini}$ and $expVOI_{replan}$) optimized for each population-based margin were generated before and after replanning. In addition, volume and coverage probabilities were also calculated.

2.6 | Statistical analysis

Pearson's correlation analysis was performed to study the correlation between cervical volume change and the daily mean displacement of the cervix or uterus. A paired *t*-test was used to analyze the statistical difference in the margin before and after replanning, as well as the volume and coverage between $expVOI_{conv}$ and expVOI or between $expVOI_{ini}$ and $expVOI_{replan}$. The significance level was set at $p < 0.05$.

3 | RESULTS

Figure 2a shows the median and interquartile range of the cervical volume trend for 11 patients. The median cervical volume fell below 50% for the first time at the 16^{th} fraction. Figure 2b,c shows the cervical volume change and displacement of the cervix and uterus, respectively. Pearson's correlation coefficients between the cervical volume change and the displacement of the cervix or uterus were −0.48 and −0.32, respectively. After the 16^{th} fraction, the cervical volume was smaller than the reference volume, except for one fraction of one patent. The correlations between the bladder or rectal volume change and displacement of the cervix or uterus are shown in Supplementary Materials.

Figure 3 shows margin sizes in the patient group. Statistical values, such as the 90^{th}, 95^{th}, and 100^{th} percentile values, are shown under the legends of R, L, A, P, S, and I. 90^{th} percentile values of patient-specific margins were used as the population-based margins. The population-based margins in (R, L, A, P, S, I) were (7, 7, 11, 6, 11, 8), and (14, 13, 27, 19, 15, 21) mm for the cervix and uterus, respectively.

Figure 4a,b summarize each individual patient's volume and overall coverage for $expVOI_{conv}$ and expVOI, respectively. For the cervix, the median volumes of $expVOI_{conv}$ and expVOI were 116.4 (range, 56.8–284.9) and 96.9 (range, 47.6–248.8) cm^3 ($p < 0.05$), respectively, whereas those of the overall coverage of $expVOI_{conv}$ and expVOI were 98 (range, 92–100) and 97 (range, 94–100) % ($p = 0.85$), respectively. For the uterus, the median values of the volumes of $expVOI_{conv}$ and expVOI were 197.6 (range, 72.7–398.7) and 251.7 (range, 104.6–491.5) cm^3 ($p < 0.05$), whereas those of the overall coverage of $expVOI_{conv}$ and expVOI were 97 (range, 76–100) and 99 (range, 79–100) % ($p < 0.05$), respectively. Figure 4c–f shows the fractional coverage of $expVOI_{conv}$ and expVOI, respectively. The median values of the fractional coverage of $expVOI_{conv}$ and expVOI were 100 (range, 66–100) and 100 (range, 59–100) % ($p = 0.65$) for the cervix, respectively. These values were 85 (range, 16–100) [%] and 100 (range, 27–100) [%] ($p < 0.05$) for the uterus, respectively.

The MR images acquired at the 16^{th} fraction, where the median cervical volume fell below 50% for the first time (Figure 2a), were used as the reference for the second plan, and replanning was performed at the 19^{th} fraction.

For the cervix, the population-based margins in (R, L, A, P, S, I) were (7, 6, 11, 6, 10, 6) and (9, 9, 11, 7, 9, 6) mm, whereas those for the uterus were (16, 12, 28, 15, 16, 17) and (13, 11, 17, 18, 13, 11) mm at the initial planning and replanning stages, respectively. No statistically significant difference was observed in the margin size between the initial and replanning stages ($p = 0.11$ for the cervix and 0.06 for the uterus). Figure 5 shows the volume and overall coverage of $expVOI_{ini}$ and $expVOI_{replan}$ in all patients. For the cervix, the median values of the volumes of $expVOI_{ini}$ and $expVOI_{replan}$ were 90.4 (range, 44.1–232.8) and 54.9 (range, 30.0–181.8) cm^3 ($p < 0.05$), whereas those of the overall coverage of $expVOI_{ini}$ and $expVOI_{replan}$ were 97 (range, 91–100) and 97 (range, 86–100) % ($p = 0.45$), respectively. For the uterus, the median values of the volumes of $expVOI_{ini}$ and $expVOI_{replan}$ were 234.8 (range, 97.5–464.8) and 155.6 (range, 80.4–369.9) cm^3 ($p < 0.05$), whereas those of the overall coverage of $expVOI_{ini}$ and $expVOI_{replan}$ were 98 (range, 81–100) and 97 (range, 62–100) % ($p = 0.32$), respectively.

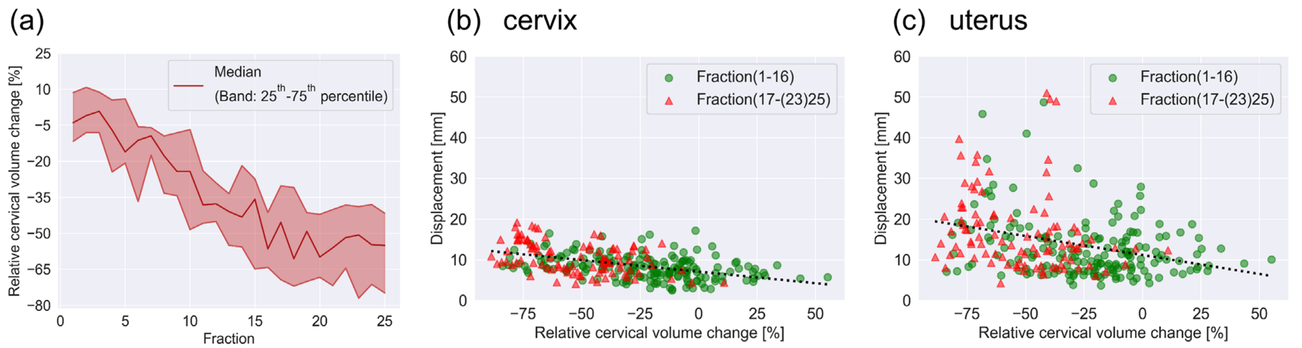

FIGURE 2 Volumetric data. (a) The trend of relative cervical volume change. Relative cervical volume change and displacement of the (b) cervix and (c) uterus. The solid lines denote regression lines.

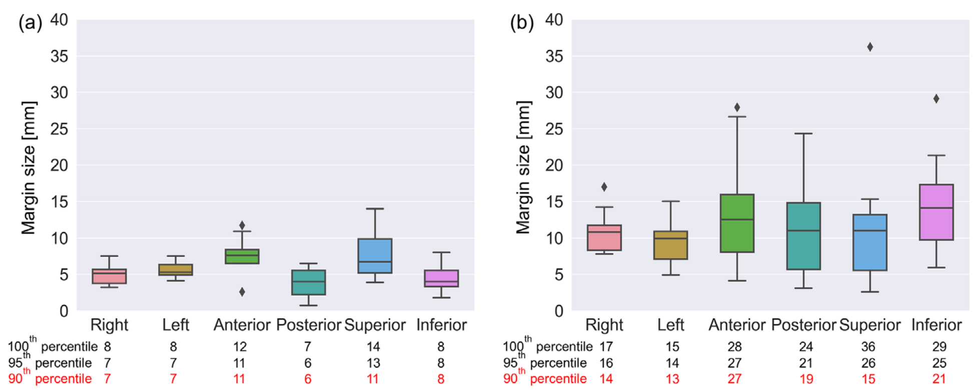

FIGURE 3 Margin size in the patient group for the (a) cervix and (b) uterus. 90th, 95th, and 100th percentile values are shown at the bottom of the figure.

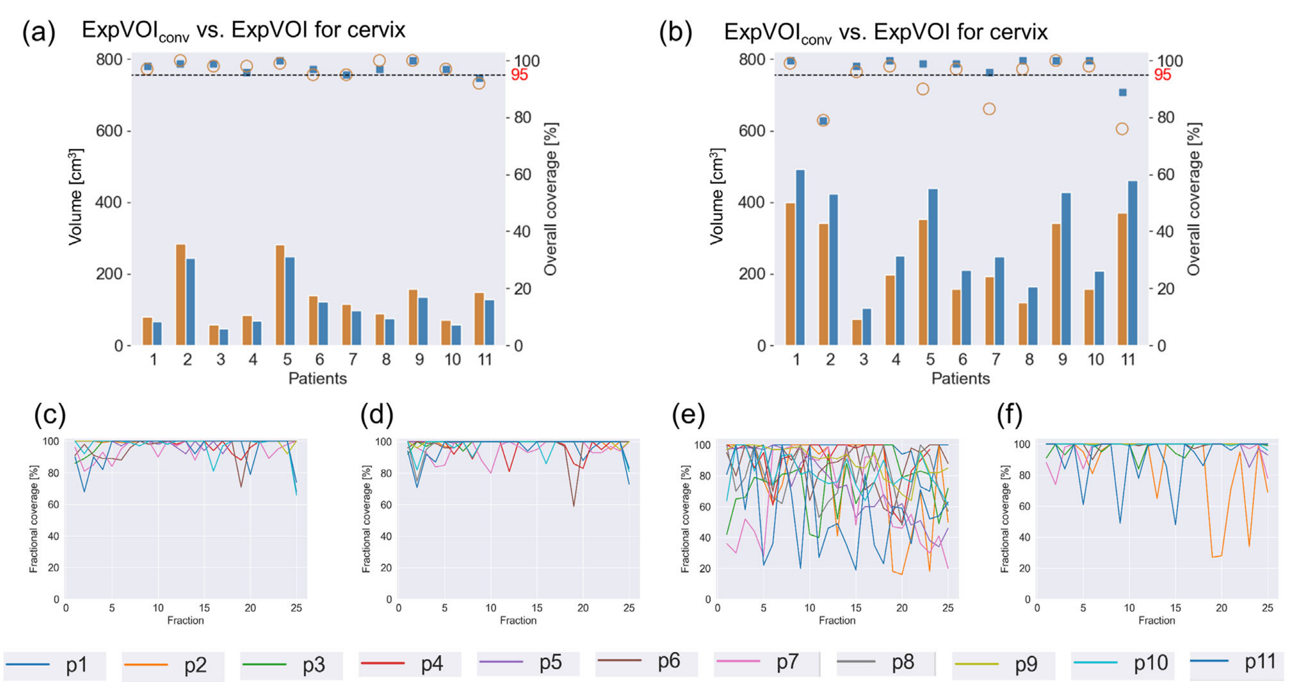

FIGURE 4 Each patient's volume and overall coverage of the expanded volume of interest (expVOI) and expVOI generated by adding conventional margins ($expVOI_{conv}$) for the (a) cervix and (b) uterus. The volumes of $expVOI_{conv}$ and expVOI are denoted by orange and blue bars, respectively, depending on the left axis. Coverage values of $expVOI_{conv}$ and expVOI are denoted by orange circles and blue squares, respectively, depending on the right axis. The 95% coverage is denoted by a dashed line. Fractional coverage values of $expVOI_{conv}$ and expVOI for the (c,d) cervix and (e,f) uterus are shown for all patients.

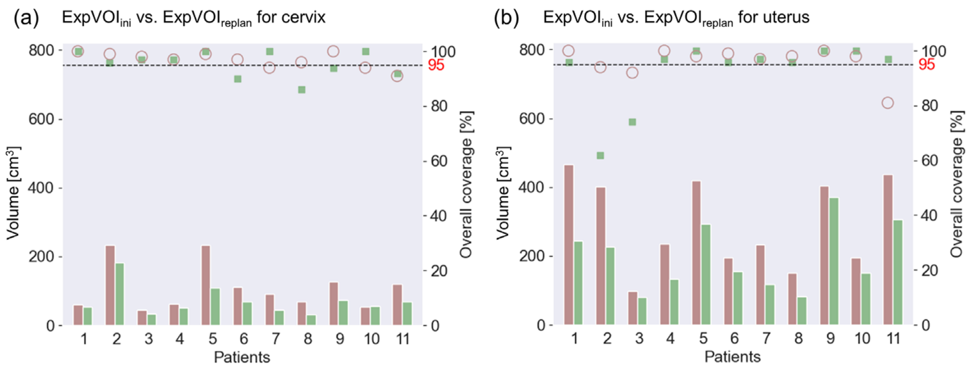

FIGURE 5 The volume and overall coverage of the expanded volume of interest by adding for each population-based margin before ($expVOI_{ini}$) and after replanning ($expVOI_{replan}$) for the (a) cervix and (b) uterus. The volumes of $expVOI_{ini}$ and $expVOI_{replan}$ are denoted by brown and green bars, respectively, depending on the left axis. The coverage values of $expVOI_{ini}$ and $expVOI_{replan}$ are denoted by brown circles and green squares, respectively, depending on the right axis. The 95% coverage is denoted by a dashed line.

4 | DISCUSSION

We computed daily interfractional cervical and uterine motions individually in 3D space using MR images. Jadon et al. summarized several reports[23] and revealed that no researchers had conducted a 3D evaluation, and daily individual assessments or high-contrast images were lacking. Therefore, the advantage of our study is achieving the exact measurement. Next, we assessed the correlation between cervical volume change and the displacement of the cervix or uterus, which showed weak negative correlations. Furthermore, the volume of the cervix was smaller than that at treatment planning after the 16th fraction, except for one fraction of one patient (Figure 2b,c), which was supported by the clinical view and other reports that the volume shrinks as the treatment progresses.[3,5,9,14] Therefore, we considered that the tumor was softened as treatment progressed, thereby facilitating the movement of the cervix and uterus (Figure 2b,c).

Table 2 summarizes the margins suggested by previous studies. We found that the margins suggested by other reports were based on a weekly assessment, lower contrast than MR images, or a 2D basis.[7–12] Several investigators did not suggest margins in six directions as they were not suitable for assessing complex variations.[8,10,11] Our margin for the cervix was smaller than the cervical or gross tumor volume (GTV) margins suggested by Collen et al. or van de Bunt et al. in all directions except for the S-I direction.[7,9] Compared to conventional margins, our margin was 2–9 [mm] smaller in the A, P, and I directions. Conversely, our margin for the uterus was equal to or larger than the conventional margins and uterine or CTV margins reported by Collen et al., van de Bunt et al., and Khan et al., except for the margins in the L, P, and S directions.[7,9,12] Because their 2D basis analysis with weekly or low-contrast images could not independently evaluate cervical and uterine variations, their variations might interfere with each other, resulting in over- and/or underestimation.

Figure 4a,c,d shows that expVOI for the cervix provided comparable coverage compared to $expVOI_{conv}$, whereas the volume of expVOI decreased by 12%–19% in all patients. Alternatively, the coverage of expVOI was significantly higher than that of $expVOI_{conv}$ in the uterus (Figure 4b,e,f). The coverage of $expVOI_{conv}$ decreased by 20% or less for three patients, and the daily variation in coverage was more notable than that in expVOI. For example, the coverage was 100% on one fraction but decreased to 18% on the next fraction for patient 2, as shown in Figure 4e. This indicated that interfractional variations were unpredictable, and hence, daily observation for interfractional movement would be required. We defined the population-based margins as the 90th percentile values of patient-specific margins. If 100th percentile values were adopted, the overall coverage and fractional coverage would improve. However, the 100th percentile values for the uterus were (17, 15, 28, 24, 36, 29) in (R, L, A, P, S, I) [mm], which would be too large for application in clinical practice. Therefore, our margins and coverage were clinically realistic.

In this study, the timing of replanning was universally picked at the 16th fraction (approximately 30 Gy) instead of personalized time points based on individual volume shrinkage, which was similar to that reported by several investigators.[5,9,14] It is crucial to closely monitor each individual volume change and trigger personalized adaptive planning decisions; however, this is beyond the scope of this study. Interestingly, although the volume of $expVOI_{replan}$ was smaller than that of $expVOI_{ini}$ for both the cervix and uterus, no significant differences were observed between the coverage of $expVOI_{ini}$ and $expVOI_{replan}$. The median volume reduction of $expVOI_{replan}$ was 37 (range, 11–56) and 30 (range, 8–50) % for the cervix and uterus at the 16th fraction, respectively. Nevertheless, the margin size should not be reduced for the cervix and uterus. As shown in Figure 2b,c, the displacement of the cervix and uterus increased as the treatment progressed. Therefore, it is likely that a margin

TABLE 2 Comparison of the measurement method and margin reported by other studies and our study.

Authors	Number of patients	Imaging frequency	Measurement		Target	Margin [mm]		
			Modality	Assessment		R-L	A-P	S-I
Collen et al.[7]	10	Daily	MVCT	2D	Cervix	8–9	17–12	15–9
					Uterus	13–13	19–19	20–19
Chan et al.[8]	20	Weekly	MRI	2D	Cervical os	10–15 (all directions)		
					Uterine funds	10–40 (all directions)		
					Uterine canal	10–12.5 (all directions)		
van de Bunt et al.[9]	20	Weekly	MRI	2D	GTV	12–11	12–14	4–8
					CTV	12–16	24–17	11–8
Wang et al.[10]	8	Biweekly (1, 3, and 5 weeks)	CT	2D	Cervix	9	10	19
					Uterus	14	32	20
Taylor et al.[11]	33	2 days	MRI	2D	CTV	7	15	15
Khan et al.[12]	50	Daily	CBCT	2D	CTV	10–10	20–20	10–10
Our study	11	Daily	MRI	3D	Cervix	7–7	11–6	11–8
					Uterus	14–13	27–19	15–21

Abbreviations: 2D, two-dimensional; 3D, three-dimensional; A, anterior; CBCT, cone-beam computed tomography; CT, computed tomography; CTV, clinical target volume; GTV, gross tumor volume; I, inferior.; L, left; MRI, magnetic resonance imaging; MVCT, megavoltage computed tomography; P, posterior; R, right; S, superior.

equivalent to that at the initial planning was required for replanning.

Nonetheless, this study has some limitations. First, delineation was conducted by a single radiation oncologist on the MR images with fixed imaging protocols. As several investigators indicated,[24,25] these factors may cause the results to change. Second, the margins and coverage were calculated based on the same patient group. Initially, margins should have been applied to a different patient group for the coverage calculation; however, it was impossible owing to the small number of cases, although a total of 273 datasets were used. Additionally, it was challenging to decide a particular confidence level and an appropriate number of patients for margin calculation. As shown in Table 2, while other studies considered various numbers of patients, none of them defined the confidence level and appropriate number of patients. Therefore, 90th percentile values of patient-specific margins were defined as population-based margins instead of confidence level. Lastly, because the intrafractional variations were not assessed, it is unclear whether the margins determined in this study compensated for intrafractional variations.[26] Intrafractional variations can also be assessed with delineated organ data acquired during beam delivery.

5 | CONCLUSION

We determined the margins and the timing of replanning through detailed daily analysis using MR images. The margins of the cervix were smaller than conventional margins and the margins suggested by other studies in some direction, while the margins of the uterus were larger in almost all directions. The timing of replanning was determined to be the 16th fraction, and the volume of $expVOI_{replan}$ decreased. However, the margin equivalent to that at the initial planning was required for replanning.

AUTHOR CONTRIBUTIONS

Yukako Kishigami and Mitsuhiro Nakamura planned the study. Yukako Kishigami performed the statistical analysis and drafted the manuscript. Yukako Kishigami, Mitsuhiro Nakamura, Megumi Nakao, and Hiroyuki Okamoto conceived the study and participated in its design and coordination. Megumi Nakao, Hiroyuki Okamoto, Ayaka Takahashi, and Hiroshi Igaki helped draft the manuscript. All authors read and approved the final manuscript.

ACKNOWLEDGMENTS

We sincerely thank all members of the Medical Physics Laboratory of Kyoto University Graduate School of Medicine and Department of Advanced Medical Physics (http://medicalphysics.hs.med.kyoto-u.ac.jp/) for their excellent technical support and valuable suggestions on this study. This research was partly supported by JSPS KAKENHI (Grant Number 22H03021).

CONFLICT OF INTEREST STATEMENT

The authors declare no conflicts of interest.

DATA AVAILABILITY STATEMENT

The data that support the findings of this study are not available.

ORCID

Hiroyuki Okamoto
https://orcid.org/0000-0001-9491-787X

REFERENCES

1. Chino J, Annunziata CM, Beriwa S, et al. Radiation therapy for cervical cancer: executive summary of an ASTRO clinical practice Guideline. *Pract Radiat Oncol*. 2020;10:220-234.
2. Lin Y, Chen K, Lu Z, et al. Intensity-modulated radiation therapy for definitive treatment of cervical cancer: a meta-analysis. *Radiat Oncol*. 2018;13:177.
3. Lim K, Chan P, Dinniwell R, et al. Cervical cancer regression measured using weekly magnetic resonance imaging during fractionated radiotherapy: radiobiologic modeling and correlation with tumor hypoxia. *Int J Radiat Oncol Biol Phys*. 2008;70:126-133.
4. Mayr NA, Wang JZ, Lo SS, et al. Translating response during therapy into ultimate treatment outcome: a personalized 4-dimensional MRI tumor volumetric regression approach in cervix cancer. *Int J Radiat Oncol Biol Phys*. 2010;76:719-727.
5. Beadle BM, Jhingran A, Salehpour M, et al. Cervix regression and motion during the course of external beam chemoradiation for cervical cancer. *Int J Radiat Oncol Biol Phys*. 2009;73:235-241.
6. Ahmad R, Hoogeman MS, Bondar M, et al. Increasing treatment accuracy for cervical cancer patients using correlations between bladder-filling change and cervix-uterus displacements: proof of principle. *Radiother Oncol*. 2011;98:340-346.
7. Collen C, Engels B, Duchateau M, et al. Volumetric imaging by megavoltage computed tomography for assessment of internal organ motion during radiotherapy for cervical cancer. *Int J Radiat Oncol Biol Phys*. 2010;77:1590-1595.
8. Chan P, Dinniwell R, Haider MA, et al. Inter- and intrafractional tumor and organ movement in patients with cervical cancer undergoing radiotherapy: a cinematic-MRI point-of-interest study. *Int J Radiat Oncol Biol Phys*. 2008;70:1507-1515.
9. van de Bunt L, Jürgenliemk-Schulz IM, de Kort GA, et al. Motion and deformation of the target volumes during IMRT for cervical cancer: what margins do we need? *Radiother Oncol*. 2008;88:233-240.
10. Wang Q, Lang J, Song Y, et al. Evaluation of intra- and interfraction movement of the cervix and the uterine body during intensity modulated radiation therapy. *Int J Radiat Oncol Biol Phys*. 2012;84:S446.
11. Taylor A, Powell ME. An assessment of interfractional uterine and cervical motion: implications for radiotherapy target volume definition in gynaecological cancer. *Radiother Oncol*. 2008;88:250-257.
12. Khan A, Jensen LG, Sun S, et al. Optimized planning target volume for intact cervical cancer. *Int J Radiat Oncol Biol Phys*. 2012;83:1500-1505.
13. Bondar L, Hoogeman M, Mens JW, et al. Toward an individualized target motion management for IMRT of cervical cancer based on model-predicted cervix-uterus shape and position. *Radiother Oncol*. 2011;99:240-245.
14. Lee CM, Shrieve DC, Gaffney DK. Rapid involution and mobility of carcinoma of the cervix. *Int J Radiat Oncol Biol Phys*. 2004;58:625-630.
15. Lim K, Stewart J, Kelly V, et al. Dosimetrically triggered adaptive intensity modulated radiation therapy for Cervical Cancer. *Int J Radiat Oncol Biol Phys*. 2014;90:147-154.
16. Stewart J, Lim K, Kelly V, et al. Automated weekly replanning for intensity-modulated radiotherapy of cervix cancer. *Int J Radiat Oncol Biol Phys*. 2010;78:350-358.
17. Seppenwoolde Y, Stock M, Buschmann M, et al. Impact of organ shape variations on margin concepts for cervix cancer ART. *Radiother Oncol*. 2016;120:526-531.
18. Oh S, Stewart J, Moseley J, et al. Hybrid adaptive radiotherapy with on-line MRI in cervix cancer IMRT. *Radiother Oncol*. 2014;110:323-328.
19. Bondar ML, Hoogeman MS, Mens JW, et al. Individualized nonadaptive and online-adaptive intensity-modulated radiotherapy treatment strategies for cervical cancer patients based on pretreatment acquired variable bladder filling computed tomography scans. *Int J Radiat Oncol Biol Phys*. 2012;83:1617-1623.
20. Heijkoop ST, Langerak TR, Quint S, et al. Clinical implementation of an online adaptive plan-of-the-day protocol for nonrigid motion management in locally advanced cervical cancer IMRT. *Int J Radiat Oncol Biol Phys*. 2014;90:678-679.
21. Nakao M, Tokuno J, Yoshikawa CT, et al. Surface deformation analysis of collapsed lungs using model-based shape matching. *Int J Comput Assist Radiol Surg*. 2019;14:1763-1774.
22. Nakao M, Kobayashi K, Tokuno J, et al. Deformation analysis of surface and bronchial structures in intraoperative pneumothorax using deformable mesh registration. *Med Image Anal*. 2021;73:102181.
23. Jadon R, Pembroke CA, Hanna CL, et al. A systematic review of organ motion and image-guided strategies in external beam radiotherapy for cervical cancer. *Clin Oncol*. 2014;26:185-196.
24. Wu HD, Mayr AN, Karatas Y, et al. Interobserver variation in cervical cancer tumor delineation for image-based radiotherapy planning among and within different specialties. *J Appl Clin Med Phys*. 2005;6:106-110.
25. Kumar S, Holloway L, Roach D, et al. The impact of a radiologist-led workshop on MRI target volume delineation for radiotherapy. *J Med Radiat Sci*. 2018;4:300-310.
26. Heijkoop ST, Langerak TR, Quint S, et al. Quantification of intra-fraction changes during radiotherapy of cervical cancer assessed with pre- and post-fraction Cone Beam CT scans. *Radiother Oncol*. 2015;117:536-541.

SUPPORTING INFORMATION

Additional supporting information can be found online in the Supporting Information section at the end of this article.

How to cite this article: Kishigami Y, Nakamura M, Nakao M, Okamoto H, Takahashi A, Igaki H. Three-dimensional assessment of interfractional cervical and uterine motions using daily magnetic resonance images to determine margins and timing of replanning. *J Appl Clin Med Phys*. 2023;24:e14073.
https://doi.org/10.1002/acm2.14073

Organ-contour-driven auto-matching algorithm in image-guided radiotherapy

Yukako Kishigami[1)], Mitsuhiro Nakamura[1)], Hiroyuki Okamoto[2)], Ayaka Takahashi[3)], Hiraku Iramina[4)], Makoto Sasaki[5)], Kohei Kawata[4)], Hiroshi Igaki[3)]

[1)]Department of Advanced Medical Physics, Graduate School of Medicine, Kyoto University, Kyoto, Japan

[2)] Radiation Safety and Quality Assurance Division, National Cancer Center Hospital, Tokyo, Japan

[3)] Department of Radiation Oncology, National Cancer Center Hospital, Tokyo, Japan

[4)] Department of Radiation Oncology and Image-Applied Therapy, Kyoto University, Kyoto, Japan.

[5)] Division of Clinical Radiology Service, Kyoto University Hospital, Kyoto, Japan

Corresponding author:

Mitsuhiro Nakamura, Ph.D. (m_nkmr@kuhp.kyoto-u.ac.jp)

Department of Advanced Medical Physics, Graduate School of Medicine, Kyoto University

53 Kawahara-cho, Shogoin, Sakyo-ku, Kyoto 606-8507, Japan

Tel: +81-75-751-4998

Short title: Organ-contour-driven auto-matching algorithm

Conflict of interests: We have no financial relationships to disclose.

Author contribution statement: YK and MN planned the study. YK performed the statistical analysis and drafted the manuscript. HO, AT, HI, SM, KK, and HI helped draft the manuscript. All authors read and approved the final manuscript.

Data sharing statement: The data that support the findings of this study are not available.

Acknowledgments: We sincerely thank all members of the Medical Physics Laboratory of Kyoto University Graduate School of Medicine, Department of Advanced Medical Physics (http://medicalphysics.hs.med.kyoto-u.ac.jp/) for their excellent technical support and valuable suggestions for this study.

Funding: This research was partly supported by JSPS KAKENHI Grant Number 22H03021.

Abstract

Purpose: This study aimed to demonstrate the potential clinical applicability of an organ-contour-driven auto-matching algorithm in image-guided radiotherapy.

Methods: This study included eleven consecutive patients with cervical cancer who underwent radiotherapy in 23 or 25 fractions. Daily and reference magnetic resonance images were converted into mesh models. A weight-based algorithm was implemented to optimize the distance between the mesh model vertices and surface of the reference model during the positioning process. Within the cost function, weight parameters were employed to prioritize specific organs for positioning. In this study, three scenarios with different weight parameters were prepared. The optimal translation and rotation values for the cervix and uterus were determined based on the calculated translations alone or in combination with rotations, with a rotation limit of ±3°. Subsequently, the coverage probabilities of the following two planning target volumes (PTV), an isotropic 5 mm and anisotropic margins derived from a previous study, were evaluated.

Results: The percentage of translations exceeding 10 mm varied from 9 to 18% depending on the scenario. For small PTV sizes, more than 80% of all fractions had a coverage of 80% or higher. In contrast, for large PTV sizes, more than 90% of all fractions had a coverage of 95% or higher. The difference between the median coverage with translational positioning alone and that with both translational and rotational positioning was 1% or less.

Conclusion: This algorithm facilitates quantitative positioning by utilizing a cost function that

prioritizes organs for positioning. Consequently, consistent displacement values were algorithmically generated. This study also revealed that the impact of rotational corrections, limited to ±3°, on PTV coverage was minimal.

Keywords: organ-contour-driven auto-matching; inter-observer variability; soft-tissue.

Introduction

Image-guided radiotherapy (IGRT) has become indispensable in the field of external beam radiotherapy owing to its effectiveness in compensating for patient positioning errors [1,2]. Among various image guidance functionalities, cone beam computed tomography (CBCT) and magnetic resonance (MR) imaging are the mainstream image guidance functionalities in IGRT, enabling soft-tissue matching [3–5]. Several investigators have demonstrated that daily soft-tissue matching resulted in smaller planning target volume (PTV) margins, outperforming bone- or skin-based matching methods [6,7]. These findings highlight the effectiveness of soft-tissue matching as a valuable approach for compensating for daily variations in target position.

However, soft-tissue matching faces several difficulties. Previous studies have consistently identified inter- and intra-observer variability as great issues in soft-tissue matching [3,8,9]. Hirose et al. emphasized the importance of considering inter-observer variability when determining the clinical target volume for PTV margins [3]. Sasaki et al. demonstrated substantial inter-observer variability and increased time requirements for soft-tissue matching in pancreatic cancer, particularly among trainees with limited experience in IGRT [8]. Furthermore, Zhang et al. conducted an analysis of the impact of inter-observer variability, underscoring its greater influence on organs at risk (OARs) than on the target in prostate cancer [9].

Current radiotherapy systems are unable to overcome the well-acknowledged challenges associated with soft-tissue matching. To address these issues, automation must be implemented. In this study, we focused on utilizing organ contours to achieve automation. Several auto-segmentation techniques have been introduced in the field of radiotherapy to assist in the delineation of targets and OARs [10,11]. Furthermore, deep learning-based auto-segmentation has demonstrated its utility in planning image and daily image segmentation [12]. While the current segmentation accuracy is imperfect, ongoing technological advancements are expected to result in improved accuracy and the eventual achievement of highly precise auto-segmentation capabilities for daily images [11,13].

The primary objective of this study is to demonstrate the potential clinical applicability of an organ-contour-driven auto-matching algorithm in IGRT, laying the groundwork for a future in which daily contouring will become a practical reality. The implementation of auto-matching technology is expected to enhance throughput and revitalize the field of radiotherapy.

Materials and methods

Patients and data preparation

For the algorithm development, eleven consecutive patients with cervical cancer who underwent MR-guided intensity-modulated radiotherapy using the ViewRay MRIdian system (ViewRay Inc., Oakwood, OH, USA) were included. The treatment was administered in 23 or 25 fractions. Detailed patient information is presented in **Table 1**. In this study, volumetric imaging was performed using true-fast imaging with a steady-state precession sequence. A total of 273 datasets were analyzed. The acquired MR scans had a slice thickness of 3 mm and pixel dimensions of 1.5 mm × 1.5 mm. Daily

MR images were co-registered with the planned MR images using the pelvic bones as a reference to determine the original position of the cervix and uterus. A single radiation oncologist manually delineated the contours of the cervix and uterus on the daily MR images. These contours were converted into the mesh file format using a commercially available system (ITEM Viewer Planning and Assistant System, ITEM Corporation, Osaka, Japan). Subsequently, the reference and daily mesh models represented by the vertices and triangular meshes were generated. The study protocol was approved by the institutional review board (approval number: 2020-556).

Cost function

In this study, the vertices of the mesh models generated from organ contours were used for auto-matching. For each treatment fraction, the vertices of the daily cervical and uterine mesh models were categorized into two groups: vertices located outside the reference model (referred to as "outside vertices") and vertices situated within the reference model (referred to as "inside vertices"). This study involved obtaining the distances between the outside or inside vertices and the surface of the reference model. These distances were denoted as "d" for the outside vertices and "D" for the inside vertices. The cost of organ A was defined as $\mathrm{Cost_A} = \mathrm{W_{out}} \sum d_i^2/i + \mathrm{W_{in}} \sum D_t^2/t$. The number of outside and inside vertices were denoted as i and t, respectively. A weight $\mathrm{W_{out}}$ was applied to the outside vertices, encouraging them to move closer to the reference position and align with the reference model. Similarly, a weight $\mathrm{W_{in}}$ was applied to the inside vertices to promote their alignment with the reference position. The cost function used in this study was the sum of the costs associated with the cervix and uterus. In this study, three scenarios with different weight parameters were prepared.

Scenario A

All weights, W_{out} and W_{in} for the cervix (W_{out_cervix} and W_{in_cervix}) and W_{out} and W_{in} for the uterus (W_{out_uterus} and W_{in_uterus}), were set to one.

Scenario B

A higher weight was assigned to the outside vertices of the cervix and uterus to bring them closer to the reference position. The weights were set as follows: (W_{out_cervix}, W_{in_cervix}, W_{out_uterus}, W_{in_uterus})=(10, 5, 10, 5).

Scenario C

The highest weight was assigned to W_{out_cervix}, and the weights were prioritized in the following order: (W_{out_cervix}, W_{in_cervix}, W_{out_uterus}, W_{in_uterus})=(10, 5, 2, 0.5). The reason why different weights were used for the cervix and uterus was to focus on the alignment of the cervix to the reference position [14].

Scenario A represented the condition in which no additional weight was employed. This scenario served as the reference to assess whether the inclusion of weight improved positioning or not. When selecting the weights, it was crucial to consider the relative size of the weight sets as the specific weight values themselves were less significant.

Optimization of cost function

In this study, the concept of dichotomy was used to determine the optimal translation and rotation values. Before the initial optimization, the original cost was calculated based on the original position determined through co-registration, using the pelvic bones as a reference. During each optimization, the calculation was performed for translational positioning only. Once translational positioning was completed, the calculation was then performed for rotational positioning, focusing solely on the rotations **(Figure 1)**.

Translational positioning

- At the first optimization of translation, the entire cervix and uterus were shifted by the distance between the centroid of the daily mesh model and reference model.
- The M^{th} translational value (M^{th} translation; $M \geq 2$) was defined as half the distance of the $(M-1)^{th}$ translation. If M^{th} translation was less than 1 mm, which represents the minimum requirement of the translational accuracy of the couch [15], M^{th} and subsequent translation was set to 1 mm.
- Following each translation, the cost was calculated and compared with that before translation. If the cost did not decrease, the cervix and uterus were returned to the position before translation.

- If the cost did not decrease after translation of 1 mm, the translational positioning process was completed. At this point, the total amount of translation from the original position was calculated. Subsequently, the rotational positioning phase commenced.

Rotational positioning

- At the first optimization of rotation, the entire cervix and uterus were rotated by 45°.
- The M^{th} rotational value ($M \geq 2$) was defined as half the rotational angle from the $(M-1)^{th}$ rotation. If M^{th} rotational angle was less than 0.5°, which represents the minimum requirement of the rotational accuracy of the couch [15], M^{th} and subsequent rotational angle was set to 0.5°.
- Following each rotation, the cost was calculated and compared with that before rotation. If the cost did not decrease, the cervix and uterus were returned to the position before rotation.
- If the cost did not decrease after rotation of 0.5°, the rotation positioning process was completed. At this point, the total rotation from the position where translational positioning was completed was then calculated.

The flow of optimization was illustrated in **Figure 2**.

Calculation of PTV coverage after optimization

In addition to the primary focus on developing the algorithm, we secondarily explored its impact on PTV coverage. Following each optimization for the three weight sets, the positions of the cervix and uterus were adjusted based on the displacements calculated from either translational positioning alone or both translational and rotational positioning. Subsequently, the coverage probabilities of the PTV were assessed for all eleven patients. For rotational positioning, the rotation limit was set to 3°, which corresponds to the allowable couch rotation tolerance at our institution. The coverage was assessed by determining the ratio of vertices from the daily cervical and uterine shape models located within the PTV to the total number of vertices outside the PTV. The PTV margins used in this study were as follows: (1) an isotropic 5 mm (PTV_{iso}) and (2) anisotropic (right (R), left (L), anterior (A), posterior (P), superior (S), inferior (I)) margins of (5, 5, 15, 15, 10, 10) mm for the cervix and (10, 10, 20, 20, 15, 15) mm for the uterus (PTV_{aniso}). The anisotropic margins of the uterus were derived from a previous study [16]. For the cervix, the margins were defined as 5 mm smaller than the uterine margins.

Statistical analysis

To evaluate the statistical differences in translation and rotation among scenarios A, B, and C, a paired *t*-test was utilized. Bonferroni correction was applied for multiple comparisons. Additionally, the PTV coverage with both translational positioning alone and combined translational and rotational positioning was also analyzed using *t*-tests. The significance level was set at 0.05. The calculation was done by Microsoft Excel 2019.

Experiment environment

All processes in this study were carried out on a desktop computer equipped with a graphics processing unit (CPU, Intel (R) with 3.00 GHz; RAM, 256 GB; GPU, NVIDIA RTX A5000) running CUDA 11.4 and Python 3.8.10.

Results

The amount of translational and rotational corrections

The percentage of translations exceeding 10 mm varied depending on the scenario **(Figure 3)**. The posterior and superior directions exhibited higher frequencies of these occurrences. In scenarios A and B, translations exceeding 10 mm were observed in 14% of all fractions in the posterior direction, whereas in the superior direction, the corresponding percentages were 18%. In scenario C, translations exceeding 10 mm accounted for 11 and 9% of all fractions in the posterior and superior directions, respectively. In contrast, translations exceeding 10 mm were only required in 0.4% of all fractions (one out of 273 fractions) for the right and left directions in scenarios A and B. Conversely, no fractions in scenario C exhibited translations exceeding 10 mm. Significant differences were observed in the anterior between scenarios A and C and superior directions between scenarios B and C and between scenarios A and C ($p<0.05$), although larger translational corrections were required in scenarios A and B than in scenario C. However, no significant differences were observed in translations in any of the six directions between scenarios A and B.

In terms of rotation, a consistent trend was observed across all scenarios **(Figure 4)**. The largest rotation was observed in the pitch axis, with median values (interquartile range) of -3.8 (-14.0–

5.6), -3.8 (-11.2–5.6), and -0.7 (-10.8–5.5) for scenarios A, B, and C, respectively. Conversely, the median and interquartile ranges for the yaw and roll axes were zero in all scenarios.

PTV coverage

Figure 5 shows the results of PTV coverage for scenarios A, B, and C. The PTV_{iso} had a coverage of 80% or higher for more than 80% of all fractions. In contrast, PTV_{aniso} had a coverage of 95% or higher for more than 90% of all fractions. While significant differences were observed (p<0.05), the difference between the median coverage with translational positioning alone and that with both translational and rotational positioning was 1% or less.

Among scenarios A, B, and C, scenarios A and B exhibited higher coverage for both PTV_{iso} and PTV_{aniso} than that of scenario C. However, a few outliers with lower coverage were observed for PTV_{iso}. In all scenarios, 8–16% of all fractions exhibited less than 80% coverage for PTV_{iso}, regardless of rotational correction. Conversely, less than 1% of all fractions had less than 80% coverage for PTV_{aniso}.

Discussion

Inter-observer variability

As shown in supplementary materials, regarding translation, the standard deviation exceeded 5 mm for 4% of the entire dataset, regardless of the direction. With respect to rotation, the standard deviation exceeded 3° for 6% of the entire dataset, regardless of the axis. This study also observed inter-observer variability, consistent with findings from previous studies [3,8,9,17–19]. These findings emphasize the need for auto-matching techniques to minimize inter-observer variability and achieve consistent soft-tissue matching.

Validity of the calculated translations by the algorithm

Although co-registration based on the pelvic bones was performed, translations exceeding 10 mm were still observed in specific directions across all weight sets. This highlights the inherent variability of the cervix and uterus, as discussed in previous studies [16,20–22]. Translations exceeding 10 mm were more frequently observed in the posterior and superior directions, whereas smaller translations were observed in the right and left directions, consistent with previous findings [23,24]. Thus, the translations calculated using the algorithm were considered valid.

Clinical significance of the displacement calculated by the algorithm

First, we discuss the findings regarding the correction of the translational component. Among the three scenarios used, scenarios A and B placed greater emphasis on correcting the position of the uterus than scenario C. As a result, adjustments were more evident in the anterior, posterior, and superior directions. This observation can be attributed to the fact that the uterus exhibits greater mobility than the cervix [24].

Next, regarding the correction of the rotational components, a pitch of 3° or higher was necessary in several fractions **(Figure 4)**. However, our hospital imposes a limit of 3° for couch rotation for safety reasons. Consequently, adequate rotational corrections may be unattainable in certain clinical scenarios. Conversely, minimal rotational movement of the cervix and uterus was observed along the yaw and roll axes, with a median value of 0. This highlights the importance of incorporating anisotropic margins to compensate for the pitch rotation. Scenario C, which prioritized the cervix over the uterus, yielded the lowest median pitch value. This indicates that addressing uncertainties related to the uterus requires substantial attention to correct pitch rotations.

Impact of the algorithm on PTV coverage

In this study, the impact of the developed algorithm was secondarily evaluated in terms of PTV coverage. In scenarios A and B, we aimed to position the cervix and uterus equally within the PTV. However, some outliers were observed **(Figure 5)**, indicating that the uterus had different shapes compared to the reference position and was largely located outside the PTV **(Figure 6)**. Priority was given to align the uterus closer to the reference position, but as a result, the cervix position deviated from the reference position. Thus, when the uterus has a different shape or position than the reference, it may be necessary to prioritize the alignment of a target with higher malignancy, the cervix rather than the uterus (in this context), or further expand the margin.

The impact of rotational corrections limited to ±3° on PTV coverage was minimal for PTV_{aniso}

(Figure 5). As mentioned previously, rotational corrections of 3° or more were deemed critical in certain fractions, implying that corrections below 3° may have a negligible effect. Furthermore, PTV_{iso} exhibited instances of insufficient coverage, even after correcting for rotational components. Therefore, precise margin settings are crucial to compensate for the rotational components of cervical cancer.

Importance of organ-driven auto-matching

Our approach algorithmically yields consistent displacement values. The integration of auto-matching technology is pivotal for mitigating inter-observer variability. Additionally, it offers the potential to minimize the risk of irradiating incorrect areas due to misidentification. This aspect becomes particularly critical in cases such as spinal stereotactic body radiation therapy, where structures resembling the target can complicate the visual identification of the precise irradiation area. These challenges increase the possibility of erroneous irradiation of incorrect targets. The utilization of the organ-contour-driven auto-matching algorithm presents a valuable solution for mitigating the risk of mis-irradiation caused by misrecognition. This advanced approach elevates the safety standards of radiotherapy and contributes to its progress. By diminishing inter-observer variability and enhancing the precision of target identification, auto-matching technology ensures treatments that are more accurate and dependable. Ultimately, this brings benefits to both patients and healthcare professionals, fostering improved radiotherapy outcomes.

Limitations

In this study, there were four limitations that warranted careful consideration. Firstly, the algorithm relies on organ contours for its function. Although auto-contouring technology has made great progress in recent years and has become feasible [11,13], its accuracy is imperfect. However, as mentioned above, it is anticipated that this challenge will be overcome in the near future and that the algorithm can be applied in conjunction with advanced contouring technology to reduce inter-observer variability and minimize mis-irradiation. Furthermore, the emergence of real-time auto-segmentation offers promising prospects for further enhancing the efficacy of this algorithm. The integration of real-time auto-segmentation has the potential to improve the overall performance and reliability of the algorithm, contributing to more precise and accurate patient positioning during radiotherapy. Secondly, the absence of ground truth makes it uncertain whether the algorithm is producing accurate results. Nevertheless, this mirrors the situation encountered in clinical practice. Although some outliers were observed **(Figure 5)**, it was determined that they resulted from considerable changes in the position of the uterus. However, in all other cases, visual evaluation confirmed that the daily cervix and uterus are consistently more centrally located within the PTV, indicating no major issues. Third, the weight sets presented in this study were arbitrarily chosen, and it is uncertain whether they are suitable for matching with other diseases. When applied clinically, it is preferable for users to determine weight sets based on their facility's background and treatment policies, considering the specific disease. Finally, the algorithm-based soft-tissue matching calculation typically consumed around 10 min. Two primary factors significantly influenced the calculation time. One was the number of vertices in the mesh model for which, we did not set an upper limit in this study. Therefore, implementing an upper limit on the number of vertices would enhance efficiency and reduce calculation time. The other factor was the computational environment. However, with advancements in computer technology, the calculation time is expected to decrease significantly.

Conclusion

We proposed the organ-contour-driven auto-matching algorithm and demonstrated its potential clinical applicability in IGRT. This algorithm facilitates quantitative positioning by utilizing a cost function that prioritizes organs for positioning. Consequently, consistent displacement values were algorithmically generated. Additionally, we also found that the impact of rotational corrections, limited to ±3°, on PTV coverage was minimal when the PTV margins were large enough to compensate for the variability of cervix and uterus.

References

1. Tsai J S, Micaily B, Miyamoto C. Optimization and quality assurance of an image-guided radiation therapy system for intensity-modulated radiation therapy radiotherapy. *Med Dosim.* 2012;37:321-333. doi: 10.1016/j.meddos.2011.11.006.
2. Tejpal G, Jaiprakash A, Susovan B, et al. IMRT and IGRT in head and neck cancer: Have we delivered what we promised? *Indian J Surg Oncol* 2010;1:166-185. doi: 10.1007/s13193-010-0030-x.
3. Hirose T, Arimura H, Fukunaga J, et al. Observer uncertainties of soft tissue-based patient positioning in IGRT. *J Appl Clin Med Phys* 2020;21:79-81. doi: 10.1002/acm2.12817.
4. Sritharan K, Tree A. MR-guided radiotherapy for prostate cancer: state of the art and future perspectives. *Br J Radiol* 2022;95:20210800. doi: 10.1259/bjr.20210800.
5. Boda-Heggemann J, Lohr F, Wenz F, et al. kV cone-beam CT-based IGRT: a clinical review. *Strahlenther Onkol* 2011;187:284-291. doi: 10.1007/s00066-011-2236-4.
6. Rossi M, Boman E, Skyttä T, et al. Dosimetric effects of anatomical deformations and positioning errors in VMAT breast radiotherapy. *J Appl Clin Med Phys* 2018;19:506-516. doi: 10.1002/acm2.12409.
7. Foroudi F, Pham D, Bressel M, et al. Bladder cancer radiotherapy margins: a comparison of daily alignment using skin, bone or soft tissue. *Clin Oncol (R Coll Radiol)* 2012;24:673-681. doi: 10.1016/j.clon.2012.06.012.

8. Sasaki M, Nakamura M, Ashida R, et al. Assessing target localization accuracy across different soft-tissue matching protocols using end-exhalation breath-hold cone-beam computed tomography in patients with pancreatic cancer. *J Radiat Res* 2023;048. doi: 10.1093/jrr/rrad048.
9. Zhang X, Wang X, Li X, et al. Evaluating the impact of possible interobserver variability in CBCT-based soft-tissue matching using TCP/NTCP models for prostate cancer radiotherapy. *Radiat Oncol* 2022;17:62. doi: 10.1186/s13014-022-02034-1.
10. Wang Z, Chang Y, Peng Z, et al. Evaluation of deep learning-based auto-segmentation algorithms for delineating clinical target volume and organs at risk involving data for 125 cervical cancer patients. *J Appl Clin Med Phys* 2020;21:272-279. doi: 10.1002/acm2.13097.
11. Cardenas CE, Yang J, Anderson BM, et al. Advances in Auto-Segmentation. *Semin Radiat Oncol* 2019;29:185-197. doi: 10.1016/j.semradonc.2019.02.001.
12. Hirashima H, Nakamura M, Imanishi K, et al. Evaluation of generalization ability for deep learning-based auto-segmentation accuracy in limited field of view CBCT of male pelvic region. *J Appl Clin Med Phys* 2023;24:13912. doi: 10.1002/acm2.13912.
13. Harrison K, Pullen H, Welsh C, et al. Machine learning for auto-segmentation in radiotherapy planning. *Clin Oncol (R Coll Radiol)* 2022;34:74-88. doi: 10.1016/j.clon.2021.12.003.
14. Haie-Meder C, Pötter R, Van Limbergen E, et al. Recommendations from Gynaecological (GYN) GEC-ESTRO Working Group (I): concepts and terms in 3D image based 3D treatment planning

in cervix cancer brachytherapy with emphasis on MRI assessment of GTV and CTV. *Radiother Oncol* 2005;74:235-245. doi: 10.1016/j.radonc.2004.12.015.

15. Klein EE, Hanley J, Bayouth J, et al. Task Group 142 report: quality assurance of medical accelerators. *Med Phys* 2009;36:4197-4212. doi: 10.1118/1.3190392.

16. Khan A, Jensen LG, Sun S, et al. Optimized planning target volume for intact cervical cancer. *Int J Radiat Oncol Biol Phys* 2012;83:1500-1505. doi: 10.1016/j.ijrobp.2011.10.027.

17. Hughes GN, Gateño J, English JD, et al. There is variability in our perception of the standard head orientation. *Int J Oral Maxillofac Surg* 2017;45:1512-1516. doi: 10.1016/j.ijom.2017.04.023.

18. Oechsner M, Chizzali B, Devecka M, et al. Interobserver variability of patient positioning using four different CT datasets for image registration in lung stereotactic body adiotherapy. *Srahlenther Onkol* 2017;193:831-839. doi: 10.1007/s00066-017-1184-z

19. Levegrün S, Pöttgen C, Jawad JA, et al. Megavoltage computed tomography image guidance with helical tomotherapy in patients with vertebral tumors: analysis of factors influencing interobserver variability. *Int J Radiat Oncol Biol Phys* 2013;85:561-569. doi: 10.1016/j.ijrobp.2012.04.010.

20. Wang Q, Lang J, Song Y, et al. Evaluation of intra- and interfraction movement of the cervix and the uterine body during intensity modulated radiation therapy. *Int J Radiat Oncol Biol Phys* 2012;84:S446. doi: 10.1016/j.ijrobp.2012.07.1181.

21. Bondar L, Hoogeman M, Mens JW, et al. Toward an individualized target motion management for IMRT of cervical cancer based on model-predicted cervix-uterus shape and position. *Radiother Oncol* 2011;99:240-245. doi: 10.1016/j.radonc.2011.03.013.

22. Lim K, Stewart J, Kelly V, et al. Dosimetrically triggered adaptive intensity modulated radiation therapy for Cervical Cancer. *Int J Radiat Oncol Biol Phys* 2014;90:147-154. doi: 10.1016/j.ijrobp.2014.05.039.

23. Chopra S, Patidar A, Dora T, et al. Vaginal displacement during course of adjuvant radiation for cervical cancer: results from a prospective IG-IMRT study. *Br J Radiol* 2014;87:20140428. doi: 10.1259/bjr.20140428.

24. Mahantshetty U, Naga P, Nachankar A, et al. Set-up errors, organ motion, tumour regression and its implications on internal target volume-planning target volume during cervical cancer radiotherapy: Results from a prospective study. *Clin Oncol (R Coll Radiol)* 2022;34:189-197. doi: 10.1016/j.clon.2021.10.010.

Figure legends

Figure 1. Original position (a), the position after translational positioning (b), and the position after rotational positioning (c). The daily cervix, daily uterus, and PTV are represented by the red, pink, and blue structures, respectively.

Figure 2. Flow of optimization.

Figure 3. Translations for scenario A (a), B (b), and C (c) calculated by the optimization for all fractions. The red dashed line represents a translation of 10 mm.

Figure 4. Rotations for scenario A (a), B (b), and C (c) calculated by the optimization for all fractions. The red dashed lines represent a rotation of ±3°.

Figure 5. Results of PTV coverage for scenario A (a), B (b), and C (c) are presented. The coverage of PTV_{iso} and PTV_{aniso} is indicated by a blue and red rectangle, respectively. Within each rectangle, the left side represents the coverage of translational positioning only (denoted as "Trans only"), and the right side represents that of both translational and rotational positioning (denoted as "Trans and rot").

Figure 6. Comparison of the uterus position after translational positioning for a case with similar shapes (a) and with large different shapes (b), compared to the reference shapes. The daily cervix, daily uterus, and PTV are represented by the red, pink, and blue structures, respectively.

Table 1. Patient characteristics

Pt#	Age (y.o.)	Pathology	TNM	Stage	Chemo	Dose (Gy/fr)	Cx (cm^3)*1	Ut (cm^3)*1
1	63	Ad	T3bN1M0	IIIB	-	46/25	15.9	102.1
2	35	SCC	T3bN1M0	IIIB	CDDP	45/25	103.8	77.9
3	65	SCC	T1b1N0M0	IB	-	45/25	9.9	3.6
4	73	SCC	T3bN1M0	IIIB	-	46/23	15.5	27.2
5	76	SCC	T3bN1M0	IIIB	CDDP	45/25	103.5	78.9
6	67	SCC	T2bN1M0	IIB	CDDP	45/25	38.8	16.9
7	71	SCC	T2bN1M0	IIB	CBDCA	45/25	29.6	33.4
8	70	SCC	T2bN0M0	IIB	CDDP	45/25	20.3	13.6
9	47	SCC	T3bN1M0	IIIB	CDDP	45/25	46.9	82.9
10	88	SCC	T1b1N0M0	IB	-	45/25	13.7	21.7
11	44	SCC	T3bNxM0	IIIB	CBDCA	45/25	45.0	91.2

Abbreviations: Pt# = patients; Ad = adenocarcinoma; SCC = squamous cell carcinoma; Chemo = chemotherapy; CDDP = cisplatin; CBDCA = carboplatin; Cx = cervix; Ut = uterus.

*1: Volume at treatment planning (cm^3)

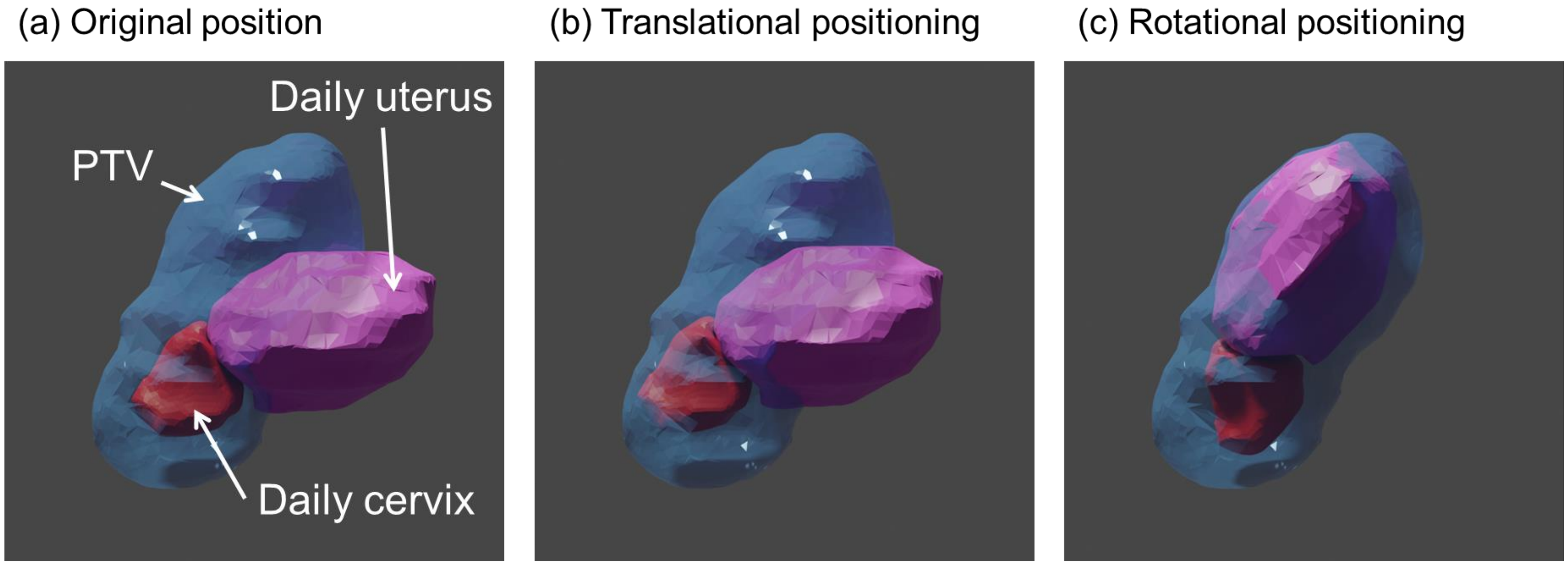

Figure 1. Original position (a), the position after translational positioning (b), and the position after rotational positioning (c). The daily cervix, daily uterus, and PTV are represented by the red, pink, and blue structures, respectively.

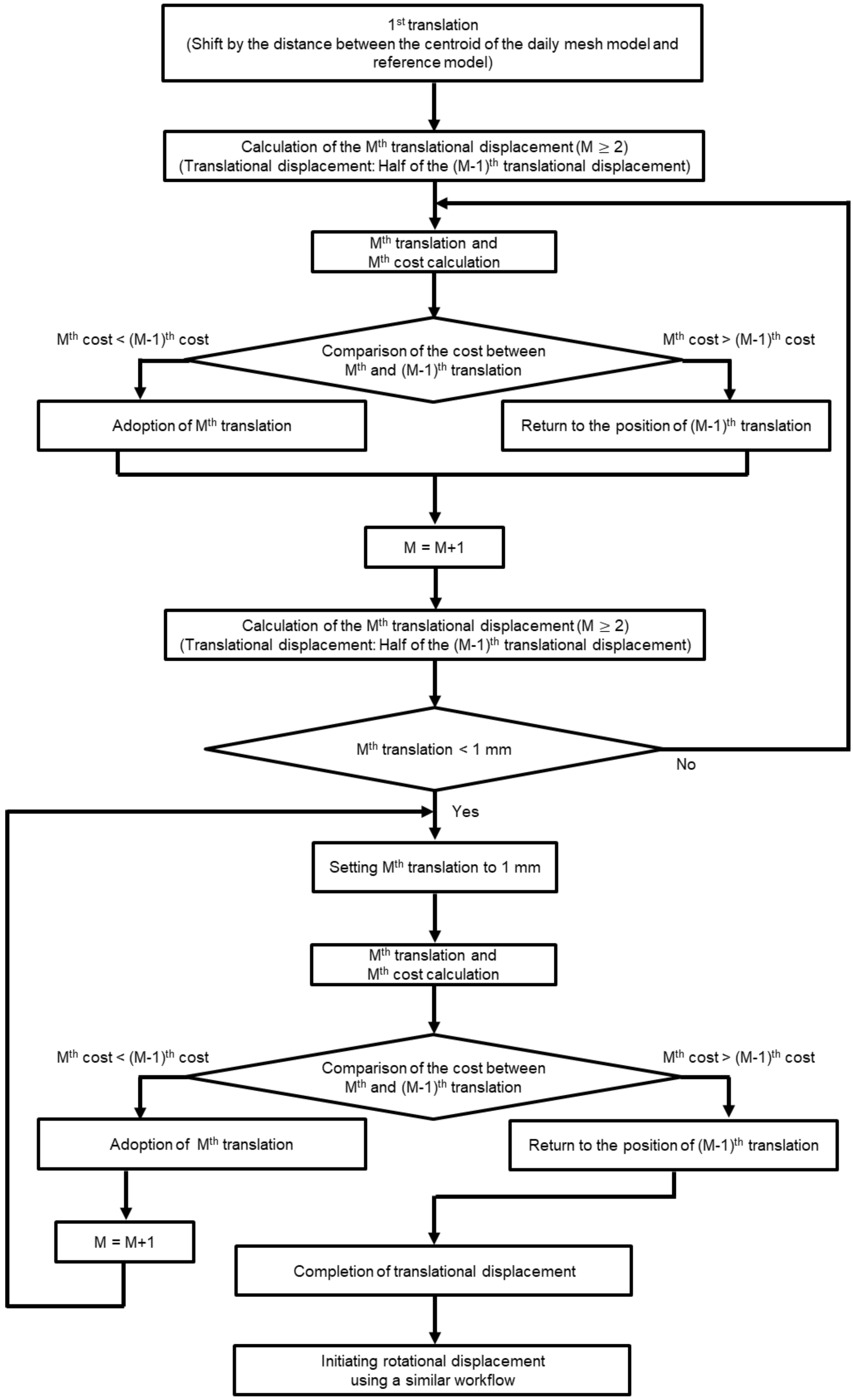

Figure 2. Flow of optimization.

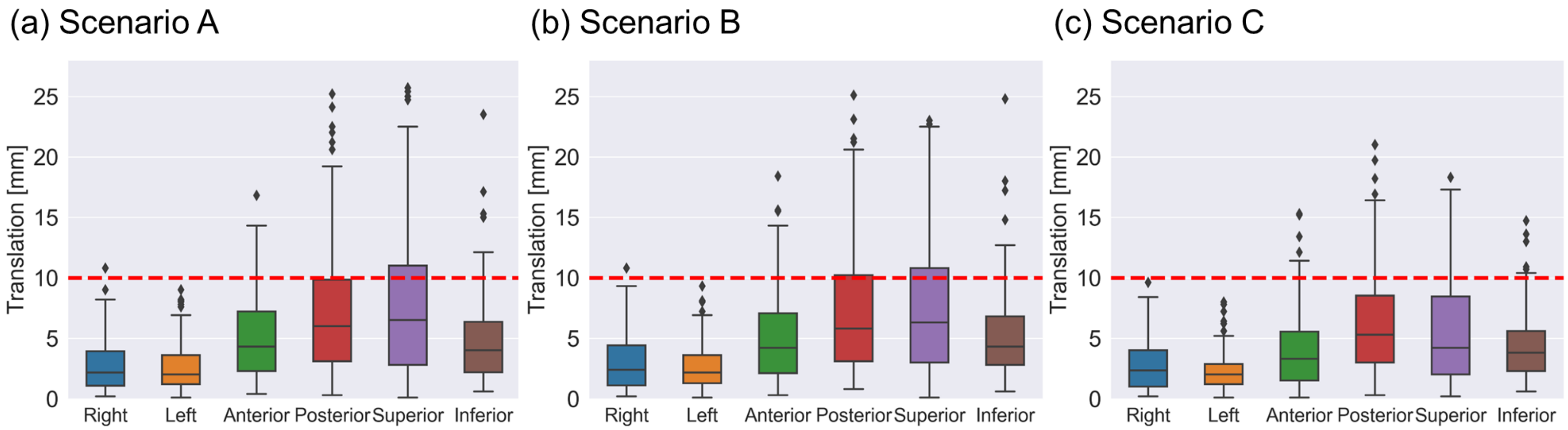

Figure 3. Translations for scenario A (a), B (b), and C (c) calculated by the optimization for all fractions. The red dashed line represents a translation of 10 mm.

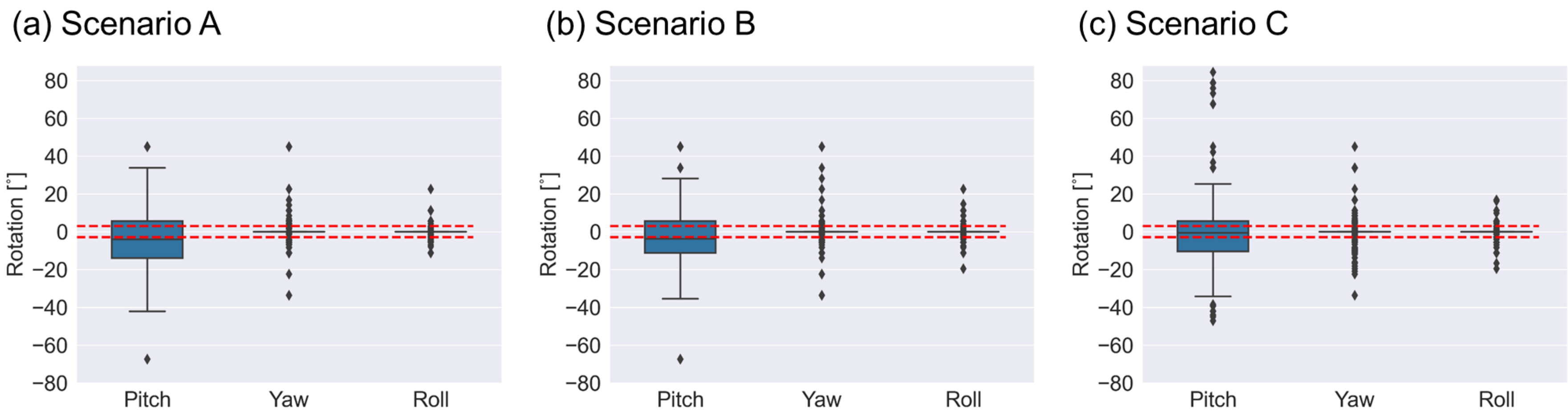

Figure 4. Rotations for scenario A (a), B (b), and C (c) calculated by the optimization for all fractions. The red dashed lines represent a rotation of ±3°

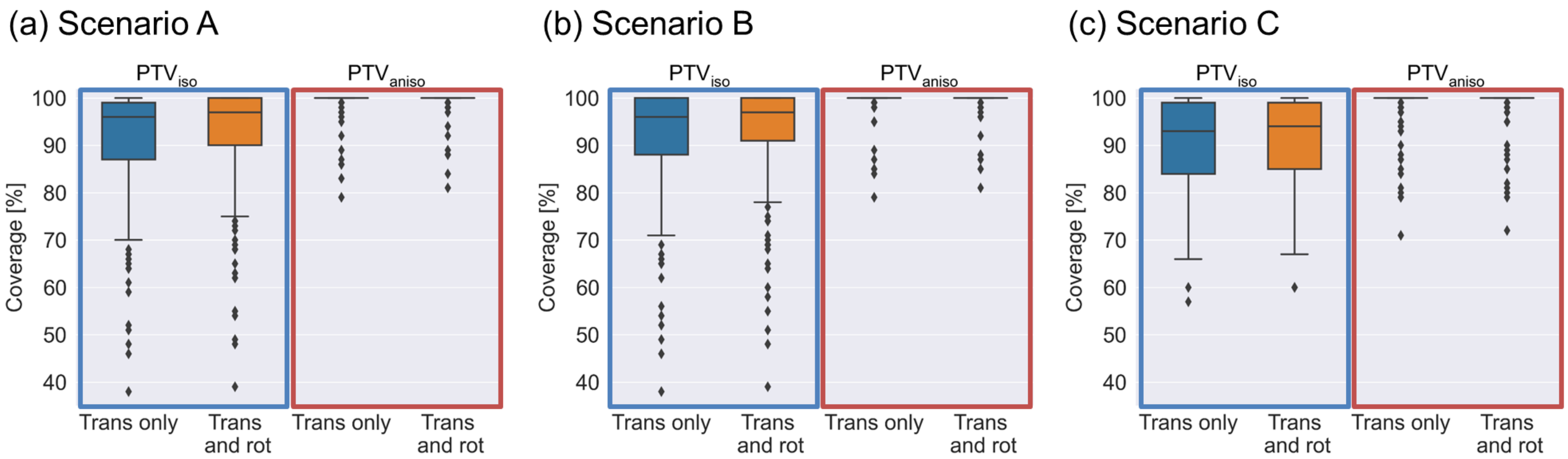

Figure 5. Results of PTV coverage for scenario A (a), B (b), and C (c) are presented. The coverage of PTV_{iso} and PTV_{aniso} is indicated by a blue and red rectangle, respectively. Within each rectangle, the left side represents the coverage of translational positioning only (denoted as "Trans only"), and the right side represents that of both translational and rotational positioning (denoted as "Trans and rot").

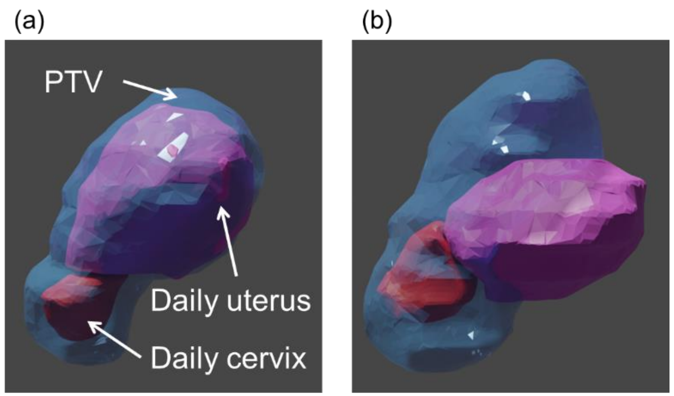

Figure 6. Comparison of the uterus position after translational positioning for a case with similar shapes (a) and with large different shapes (b), compared to the reference shapes. The daily cervix, daily uterus, and PTV are represented by the red, pink, and blue structures, respectively.

Supplementary materials

Materials and methods

Assessment of inter-observer variability

As previously mentioned, inter-observer variability was identified in previous studies [1–3]. In this preliminary study, we further investigated inter-observer variability that might arise when performing soft-tissue matching with our facility's personnel and equipment. The soft tissue matching was conducted by three medical physicists and two radiation therapists. The three physicists had different levels of experience with 18, 8, and 3 years of experience, respectively. Similarly, the two radiation therapists had varying levels of experience with 13 and 3 years of experience, respectively. Soft-tissue matching was performed on six patients with pancreatic cancer, totaling 29 fractions. Planning CT (pCT) scans were acquired under breath-holding conditions using a 64-slice CT scanner (SOMATOM Definition AS; Siemens Healthineers, Erlangen, Germany). The CT scans were acquired at 120 kV, with a slice thickness and slice interval of 2.0 mm and field of view of 500 mm. Daily CBCT images were acquired using a Varian Ethos system (Varian Medical Systems, Palo Alto, CA, USA). The CBCT scans were performed at 125 kV with a slice thickness of 2.0 mm and scan diameter of 492 mm. The pCT and daily CBCT images were aligned based on the bony structures, and the participants were instructed to align the gross tumor volume (GTV) by performing translational and rotational adjustments of the daily CBCT images on the pCT source images. No movement limitations were imposed, and only the contour of the GTV delineated on the pCT was displayed. Inter-observer variability was defined as the standard deviation of each subject's positioning, calculated for each fraction of translation and rotation.

Results

Assessment of inter-observer variability

Supplementary Figure 1 illustrates the results of inter-observer variability for translation and rotation. For translation, the standard deviation exceeded 2, 3, and 5 mm for 13, 5, and 4% of the entire dataset, respectively, regardless of the direction. For rotation, the standard deviation exceeded 2 and 3° for 13 and 6% of the entire dataset, respectively, regardless of the axis.

References

1. Hirose T, Arimura H, Fukunaga J, et al. Observer uncertainties of soft tissue-based patient positioning in IGRT. *J Appl Clin Med Phys* 2020;21:79-81. doi: 10.1002/acm2.12817.
2. Sasaki M, Nakamura M, Ashida R, et al. Assessing target localization accuracy across different soft-tissue matching protocols using end-exhalation breath-hold cone-beam computed tomography in patients with pancreatic cancer. *J Radiat Res* 2023;048. doi: 10.1093/jrr/rrad048.

3. Zhang X, Wang X, Li X, et al. Evaluating the impact of possible interobserver variability in CBCT-based soft-tissue matching using TCP/NTCP models for prostate cancer radiotherapy. *Radiat Oncol* 2022;17:62. doi: 10.1186/s13014-022-02034-1.

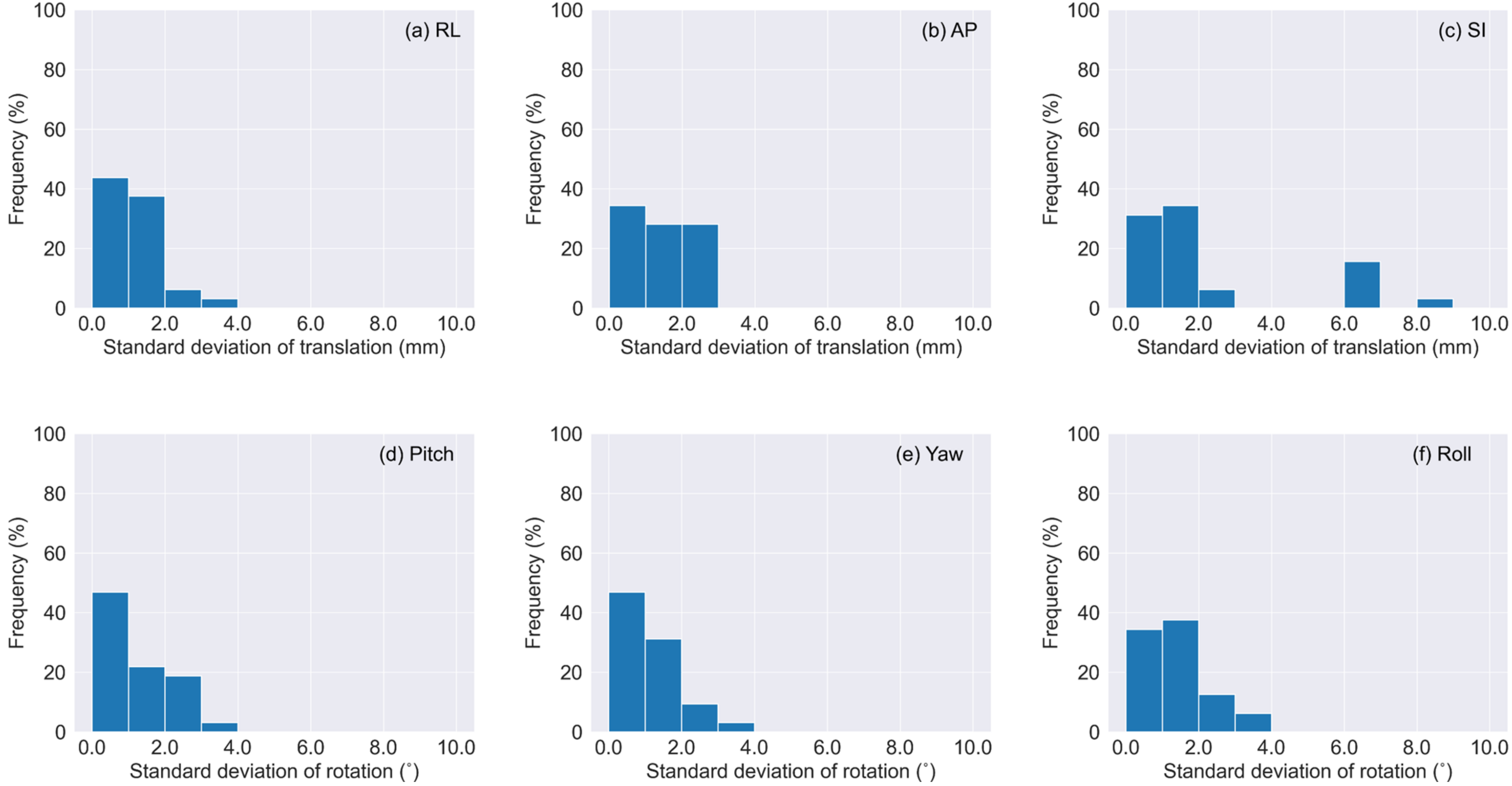

Supplementary Figure 1. The standard deviation results for translation ((a)-(c)) and rotation ((d)-(f)) representing inter-observer variability.